Local anesthetic inhibition of a bacterial sodium channel

Sora Lee,[1,2] Samuel J. Goodchild,[1,2] and Christopher A. Ahern[1,2]

[1]Department of Anesthesiology, Pharmacology, and Therapeutics and [2]Department of Cellular and Physiological Sciences, University of British Columbia, Vancouver, British Columbia V6T 1Z3, Canada

Recent structural breakthroughs with the voltage-gated sodium channel from *Arcobacter butzleri* suggest that such bacterial channels may provide a structural platform to advance the understanding of eukaryotic sodium channel gating and pharmacology. We therefore set out to determine whether compounds known to interact with eukaryotic Na_Vs could also inhibit the bacterial channel from *Bacillus halodurans* and NaChBac and whether they did so through similar mechanisms as in their eukaryotic homologues. The data show that the archetypal local anesthetic (LA) lidocaine inhibits resting NaChBac channels with a dissociation constant (K_d) of 260 µM, and channels displayed a left-shifted steady-state inactivation gating relationship in the presence of the drug. Extracellular application of QX-314 to expressed NaChBac channels had no effect on sodium current, whereas internal exposure via injection of a bolus of the quaternary derivative rapidly reduced sodium conductance, consistent with a hydrophilic cytoplasmic access pathway to an internal binding site. However, the neutral derivative benzocaine applied externally inhibited NaChBac channels, suggesting that hydrophobic pathways can also provide drug access to inhibit channels. Alternatively, ranolazine, a putative preopen state blocker of eukaryotic Na_Vs, displayed a K_d of 60 µM and left-shifted the NaChBac activation-voltage relationship. In each case, block enhanced entry into the inactivated state of the channel, an effect that is well described by a simple kinetic scheme. The data suggest that although significant differences exist, LA block of eukaryotic Na_Vs also occurs in bacterial sodium channels and that NaChBac shares pharmacological homology to the resting state of vertebrate Na_V homologues.

The Journal of General Physiology

INTRODUCTION

The initial discovery and characterization of a voltage-gated sodium channel from *Bacillus halodurans* (NaChBac) have held promise that these channels may serve as functional homologues of the eukaryotic sodium channels that control action potential firing in the excitable cells of nerve and muscle (Ren et al., 2001). Such bacterial sodium channels have generated interest for their interrogation via structural approaches that are currently out of reach for the analysis of mammalian Na_Vs but could aid significantly in closing conceptual gaps that persist in the understanding of the eukaryotic sodium channel gating, selectivity, and pharmacology. This possibility has been partially realized with the structure of the sodium channel from *Arcobacter butzleri* (Payandeh et al., 2011), yet many questions persist regarding the structural and functional conservation between bacterial progenitors and their eukaryotic Na_V descendants and whether NaChBac represents a bona fide pharmacological model to advance eukaryotic Na_V drug design and understanding.

NaChBac and eukaryotic Na_Vs selectively allow the transmembrane conductance of sodium ions and share a common fourfold domain arrangement around a central axis that defines the permeation pathway. Each domain contains six segments (S1–S6), with S1–S4 forming a voltage-sensing module, pore S5–S6 segments that comprise the selectivity filter, an inner vestibule, and the S6 segments that gate the passage of ions. In response to membrane depolarization, the S4 segments of NaChBac carry their positively charged Arg and Lys residues in an outward trajectory (Blanchet and Chahine, 2007), similar to mammalian Na_V channels (Yang et al., 1996). Despite these intrinsic similarities, considerable differences exist. For one, NaChBac is a homotetramer, whereas eukaryotic Na_Vs are encoded by a single polypeptide that forms a heterotetramer tethered by cytoplasmic linkers. One obvious outcome of this design posits that eukaryotic Na_Vs are likely to engage in asymmetrical chemical contacts with ions and cationic blockers that occupy the pore. For instance, four glutamate side chains form the NaChBac Na^+ ion–selective filter but can easily be converted to become Ca^{2+} selective (Yue et al., 2002), suggesting that bacterial sodium channels may as easily serve as models for calcium channel selectivity and permeation. NaChBac channels also lack key cytoplasmic domains that support eukaryotic Na_V fast inactivation, namely the cytoplasmic DIII–IV linker and the cytoplasmic carboxyl terminus (Ren et al., 2001), structural absences that likely underlie the significant delayed entry

Correspondence to Christopher A. Ahern: chrisahern@gmail.com

Abbreviations used in this paper: LA, local anesthetic; SSI, steady-state inactivation.

The Rockefeller University Press $30.00
J. Gen. Physiol. Vol. 139 No. 6 507–516
www.jgp.org/cgi/doi/10.1085/jgp.201210779

into, and recovery from, inactivated states of NaChBac channels. The mechanisms that support NaChBac inactivation are unknown but have been proposed to occur in a manner homologous to the pore rearrangement similar to C-type inactivation in potassium channels (Pavlov et al., 2005), although other mechanisms akin to activation gate "slippage" of the S6 segment remain unexplored (Shin et al., 2004).

Therapeutic sodium channel inhibition by local anesthetic (LA) drugs is used to calm membrane excitability that is manifest in epilepsy, cardiac arrhythmia, and painful syndromes. These amphipathic drugs contain titratable amine moieties with pKas in the physiological range, and it has been proposed that the neutral species of the drug can readily diffuse into closed channels, producing a resting or "tonic" inhibition of channel activity (Hille, 1977). Alternatively, after traversing the span of the membrane in the neutral form, the reprotonated drug can act as a charged, rapid open channel blocker from the cytoplasmic face (Kimbrough and Gingrich, 2000). Such divergent hydrophobic and hydrophilic access routes to active sites, in combination with differential drug interactions with resting and active channel conformational states, give rise to the clinically important phenomena of tonic and use-dependent channel inhibition (Schwarz et al., 1977). In the latter case, channel (over)use results in up to 10-fold higher affinity caused by enhanced drug interactions with open/inactivated channel conformations.

NaChBac shares pharmacological similarities with Ca_V channels in that both are inhibited by cadmium and dihydropyridine compounds (Ren et al., 2001), yet very little is known of the possible interactions between NaChBac and LA compounds known to inhibit eukaryotic Na_Vs. It has been suggested that etidocaine preferably blocks open NaChBac channels, but the supporting data are sparse on the details of such mechanisms (Zhao et al., 2004). Structural cues provided by *Arcobacter butzleri* suggest that large cationic drugs may occupy the channels, but it is not known whether LA drugs are capable of inhibiting the NaChBac channels once they reach the inner vestibule.

MATERIALS AND METHODS

Two-electrode voltage clamp

Voltage-clamped sodium currents were recorded with two microelectrodes using an OC-725C voltage clamp (Warner) in a standard Ringer's solution (in mM): 116 NaCl, 2 KCl, 1 $MgCl_2$, 0.5 $CaCl_2$, and 5 HEPES, pH 7.4. All recordings were performed at 20–22°C. Glass microelectrodes had resistances of 0.1–1 MΩ and were backfilled with 3 M KCl. The holding potential was −120 mV in all cases. G-V relationships were derived by plotting the isochronal tail current amplitudes (the current amplitude measured after stepping from the test potential back to a holding potential of −120 mV) as a function of the depolarizing pulse potential. All displayed current traces show the full active voltage range of G-Vs. All data are means ± SEM. The T220A mutant was transiently expressed via calcium phosphate transfection in HEK-293 cells for patch-clamp recordings. The electrode resistance was in the range of 1.0 to 1.5 MΩ, and the voltage errors resulting from series resistance was always <3 mV after compensation. Liquid junction potentials between the bath and the pipette solution were corrected. All experiments were performed at room temperature. The patch pipette contained (in mmol/L) 60 $CsCl_2$, 13 NaCl, 80 K-aspartic acid, 11 EGTA, 1 $MgCl_2$, 1 $CaCl_2$, and 10 HEPES, pH 7.2. The bath contained (in mmol/L) 150 NaCl, 2 KCl, 1.5 $CaCl_2$, 1 $MgCl_2$, and 10 HEPES, pH 7.4.

All drug stock solutions were kept at −20°C. Ranolazine and lidocaine working solutions were prepared by diluting from stock solutions, 50 mM and 200 mM, respectively, in Ringer's at room temperature. 500 mM benzocaine stock solution was made in DMSO, and it was diluted in Ringer's for appropriate working concentrations.

Homology modeling

The sequences of the pore (S5–S6 region) of NaChBac were aligned using ClustalW2 with that of the S5–S6 region of the NavAb structure (Protein Data Bank accession no. 3RVY; Payandeh et al., 2011). Two homology models of NaChBac subunits based on this alignment were generated using 3RVY chain A and B as template structures using the Swiss-Model server. The modeled subunits representing the symmetric and asymmetric subunits of the NavAb structure were then assembled to form a NaChBac tetramer by fitting the modeled subunits onto the biologically relevant NavAb tetramer structure. All structures and electrostatic surfaces are displayed using PyMol.

RESULTS

A NaChBac homology model was constructed from the recent crystal structure of the voltage-gated sodium channel from *Arcobacter butzleri* (NavAb) and is shown in Fig. 1. An alignment of the S5 and S6 segments of the two bacterial sodium channels shows strong conservation of regions of known importance for LA block, including the selectivity filter and S5 and S6 transmembrane segments. Notably, however, the NavAb "fenestrations" that are possibly guarded by an aromatic residue, Phe203, are poorly conserved in sodium channels, and this site is Leu in NaChBac channels. Nonetheless, the model suggests that both channels have well-defined cytoplasmic and alternative access routes within the transmembrane region and large internal vestibules that could accommodate blocking molecules. We first examined the effects of the amphipathic classical LA lidocaine on two-electrode voltage-clamped currents recorded from *Xenopus laevis* oocytes injected with NaChBac cRNA. NaChBac channels in this expression system displayed stable expression after 24–48 h and had similar kinetic properties and activation and inactivation steady-state behavior to channels expressed in mammalian cultures (Table 1; Ren et al., 2001). Most striking in each case for both oocyte and cultured cell expression is the apparent stability of a long-lived inactivated state of the channel once the channel had been fully inactivated. However, this issue can be partially overcome with negative holding potentials, −120 mV in the

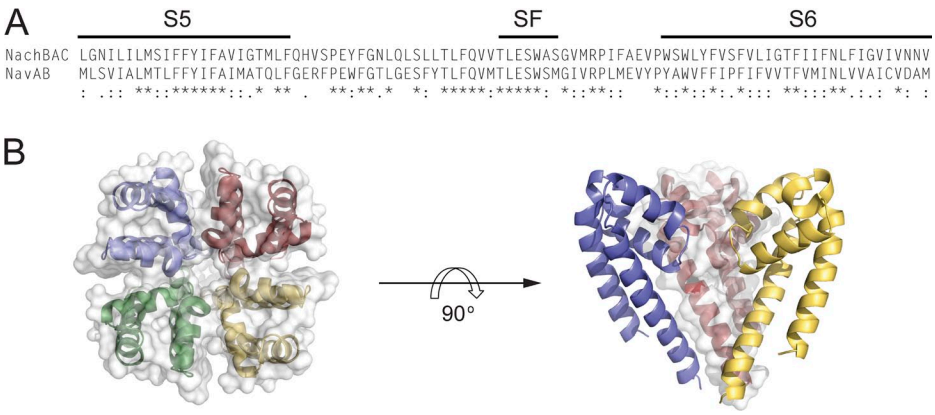

Figure 1. Homology model of NaChBac. (A) Sequence alignment of the pore region (S5–selectivity filter–S6 segments) of NaChBac aligned with NavAb. SF, selectivity filter. Stars indicate conservation, double dots show strong conservation, and single dots indicate weak conservation. (B) A homology model of the pore region of NaChBac generated based on the crystal structure of NavAb. The structure is shown with a top view (left) and a side view (right), with one monomer removed for clarity.

present case, and by using infrequent or brief test potentials where channels do not spend significant amounts of time visiting inactivated states. Fig. 2 A shows that peak current-voltage relationships for NaChBac currents display a positive reversal potential of ∼50 mV, consistent with a sodium selective pore, with a representative family of sodium currents shown in the inset. To assess the efficacy of the block by lidocaine, a concentration response curve was generated, and the mean data were fit with a Hill equation, giving an IC_{50} of 260 µM and a slope of ∼0.9 (Fig. 2 B). Each point represents the steady-state inhibition of currents produced by the application of lidocaine during repeated depolarizing pulses to −20 mV every 15 s. Under these test pulse conditions, very little current loss was seen under control drug-free conditions (not depicted). A family of normalized current traces from −120 to −20 mV in the bottom inset in Fig. 2 B demonstrates current inhibition of NaChBac currents, starting with a control trace and followed by increasing concentrations of lidocaine with values listed in the legend. To assess the time course of block and recovery, cells were held at a voltage at which NaChBac channels are tightly closed (−120 mV) during the perfusion of lidocaine into the bath. A diary plot of peak current against time is shown in Fig. 2 C, with representative current traces for the first pulse in each series displayed at the top. Oocytes were held at −120 mV for at least 1 min before the first control depolarizing pulse to minimize accumulated inactivation. However, the subsequent pulse often displayed a modestly reduced current but was then stabilized upon additional depolarizing pulses to −20 mV for 1,500 ms with 15-s intervals between pulses. The pulse protocol was stopped before a 3-min application of lidocaine to closed channels, after which the protocol was restarted. The diary plots show that channels were substantially inhibited in the first depolarization, similar to resting or tonic block of eukaryotic voltage-gated sodium channels. After 5 min of washing with Ringer's solution while holding the cells at −120 mV, depolarization pulses to −20 mV showed that block was reversible, and current levels were recovered to preblock levels. Tail current G-V and steady-state inactivation (SSI) curves were generated before and after drug exposure to lidocaine and fit with a Boltzmann function. Fig. 2 D shows that lidocaine induced an ∼10-mV left shift in SSI, signifying an increase in the stability of the inactivated state of the channel in the presence of the drug, with values for $V_{1/2}$ = −51.97 ± 1.55 mV (mean ± SEM; n = 4) and for lidocaine, $V_{1/2}$ = −62.12 ± 1.12 mV (n = 4, $P < 0.05$). The left shift in G-V was less prominent but statistically significant, displaying an ∼5-mV left shift; control $V_{1/2}$ = −26.54 ± 2.80 mV, and 1 mM lidocaine $V_{1/2}$ = −30.50 ± 2.59 mV (n = 4, $P < 0.05$).

To probe the location of the blocking site in NaChBac, we used the permanently charged membrane impermeant analogue of lidocaine, QX-314. Fig. 3 A illustrates that external application of 200 µM QX-314, in contrast to lidocaine, did not inhibit sodium current. The data show that Na^+ current density before and after the application of QX-314 was unchanged, suggesting

TABLE 1

Effects of hydrophobic and hydrophilic drugs on NaChBac activation and inactivation

	Effects on activation of NaChBac						Effects on inactivation of NaChBac					
	Ranolazine (200 µM)		Lidocaine (1 mM)		Benzocaine (1 mM)		Ranolazine (200 µM)		Lidocaine (1 mM)		Benzocaine (1 mM)	
	$V_{1/2}$	dx	$V_{1/2}$	dx	$V_{1/2}$	dx	$V_{1/2}$	dx	$V_{1/2}$	dx	$V_{1/2}$	dx
	mV	*mV*	*mV*	*mV*	*mV*	*mV*	*mV*	*mV*	*mV*	*mV*	*mV*	*mV*
Control	−19.8 ± 1.4[a]	11.1 ± 0.6[a]	−26.5 ± 2.8[a]	10.4 ± 0.4	−17.9 ± 2.1	9.8 ± 0.2	−50.8 ± 0.6[a]	6.2 ± 1.0	−52.0 ± 1.6[a]	5.9 ± 0.5	−44.7 ± 0.8[a]	7.0 ± 0.2
Drug	−32.8 ± 2.1[a]	6.2 ± 0.6[a]	−30.5 ± 2.6[a]	10.9 ± 0.8	−21.1 ± 5.9	10.0 ± 1.5	−57.9 ± 0.4[a]	6.8 ± 0.6	−62.1 ± 1.1[a]	5.8 ± 0.4	−58.9 ± 0.8[a]	6.9 ± 0.4

Mean ± SEM is given.

[a]Statistical significance was set at $P < 0.05$.

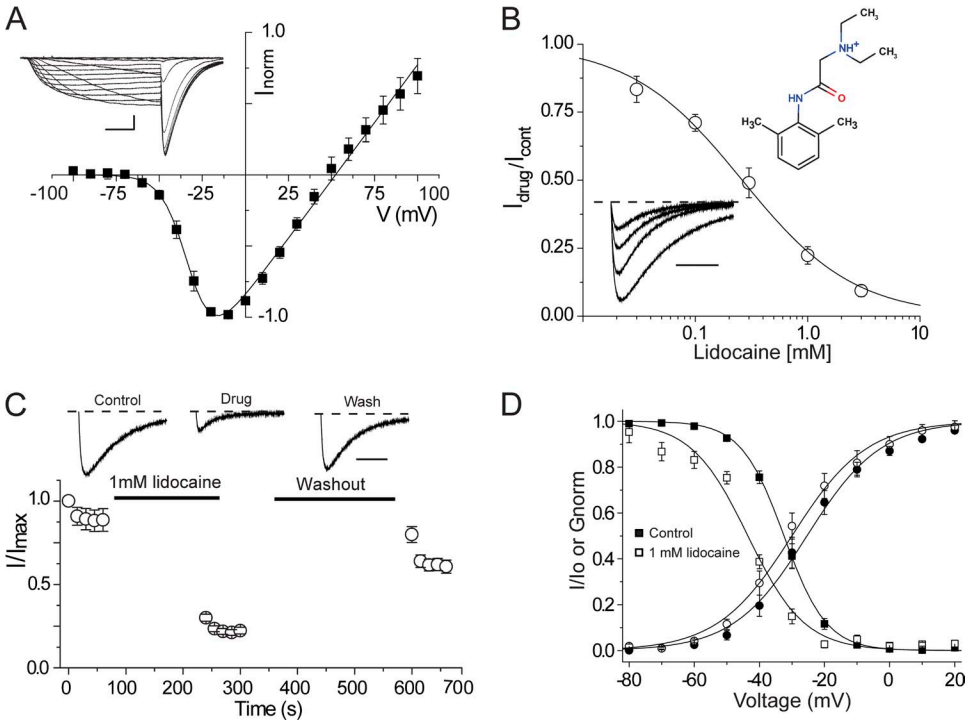

Figure 2. Effects of the LA lidocaine on NaChBac currents. (A) A current-voltage relationship curve for wild-type NaChBac is shown for *Xenopus* oocytes expressing NaChBac channels held at a holding potential of −120 mV. Currents were activated by 100 ms of depolarizing pulses from −100 to 100 mV in 10-mV increments followed by repolarization to −120 mV. n = 4. Representative current traces are shown in the inset. Bar: horizontal, 20 ms; vertical, 2 µA. (B) A concentration response curve was generated with the mean of $I_{drug}/I_{control}$ obtained from the peak currents after exposing cells to 30 µM, 100 µM, 300 µM, 1 mM, and 3 mM lidocaine. The IC_{50} for lidocaine according to the concentration response curve is ∼260 µM. Representative current traces obtained after depolarization from the holding potential −120 to −20 mV in the presence of various lidocaine concentrations (0 µM, 100 µM, 300 µM, and 1 mM) on oocytes expressing wild-type NaChBac channels are shown in the bottom inset. Currents are normalized to the peak amplitude of the control trace. The dashed line indicates the zero current level. The top inset is a chemical structure of lidocaine. n = 4. Bar, 500 ms. (C) Diary plot showing normalized peak current inhibition resulting from extracellular application of 1 mM lidocaine while holding the cells at −120 mV for 3 min. In the presence of 1 mM lidocaine, a 1,500-ms depolarizing pulse to −20 mV was performed. Depolarizing pulses were followed by a 5-min Ringer's solution wash while holding the cells at −120 mV. Representative current traces are shown with the zero current lines (dotted lines). Bar, 500 ms. (D) Conductance-voltage relationship curves are shown for control (●) and after 1 mM lidocaine exposure (○). A significant left shift ($P < 0.05$) is observed in the SSI curve after 1 mM lidocaine exposure (□) as compared with the control (■). n = 5. Error bars represent SEM.

that the blocking site is on the intracellular side of the channel, out of reach of QX-314. Consistent with this possibility, Fig. 3 B shows that when QX-314 is injected intracellularly into oocytes under voltage clamp at −120 mV, sodium current was rapidly blocked upon depolarization, suggesting access to the intracellular binding site is cytoplasmic and hydrophilic in nature. To further test this possibility, we examined the effects of extracellular benzocaine, an uncharged molecule at pH 7.4. Fig. 4 A shows that NaChBac channels could be blocked, albeit with a reduced affinity of IC_{50} of 650 µM and a Hill slope of ∼1.0. The ability of benzocaine to inhibit NaChBac currents when applied extracellularly supports a role for hydrophobic pathways for LA block in NaChBac

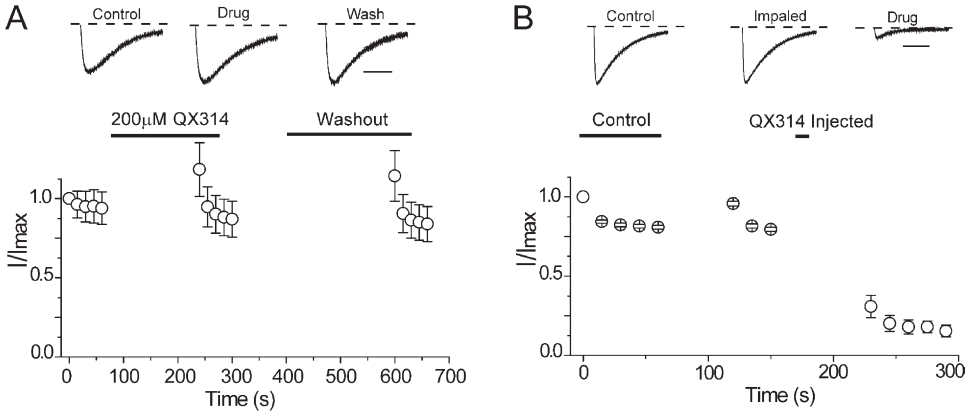

Figure 3. Evidence for an intracellular binding site. (A) Perfusion of external 200 µM QX-314 and washout as described in Fig. 2 C shows that QX-314 cannot block expressed NaChBac channels. n = 3. Representative current traces are shown with the zero current lines (dotted lines). Bar, 500 ms. (B) Intracellular injection of QX-314 solution under voltage clamp. Control pulses were performed in Ringer's solution, depolarizing from −120 to −20 mV at 15-s intervals. Cells were then impaled with the injection electrode while being held at −120 mV. Time between the last pulse of control and after impaling varies from 2 to 3 min. 30 nl of 16.7 mM QX-314 was injected at a holding potential of −120 mV to produce ∼500 µM QX-314 internal concentration. Cells were incubated in Ringer's solution for 3 min before recording. Injected QX-314 inhibited sodium currents as shown in the current trace (top). n = 6. Error bars represent SEM.

channels. Similar to lidocaine effects on gating properties, benzocaine induced a statistically significant hyperpolarizing shift in SSI curves (Table 1). Lastly, we explored the possibility that a conventional drug with a divergent structure from lidocaine, such as ranolazine, also retained the ability to block NaChBac. The data clearly show that external perfusion of ranolazine potently inhibited sodium currents compared with lidocaine, with an IC_{50} of 60 µM (Fig. 5). Similar to lidocaine and benzocaine, inhibition by ranolazine is illustrated in the diary plot in Fig. 5 C. Current inhibition was reversed after 5 min of washout with Ringer's solution at a holding potential of −120 mV. To confirm that our results were not specific to the *Xenopus* oocyte expression system, ranolazine was applied to NaChBac channels transiently transfected in HEK-293 cells under patch-clamp conditions. Here, similar to the oocyte, 200 µM ranolazine potently and reversibly inhibited channels (not depicted). In the oocyte, ranolazine induced a significant left shift in both G-V and SSI curves (Fig. 5 D). The $V_{1/2}$ of G-V curves after ranolazine exposure was −32.8 ± 2.1 mV compared with a $V_{1/2}$ of control of −19.8 ± 1.4 mV (n = 4, P < 0.05). The hyperpolarizing left shift in the SSI curve is slightly less prominent with ∼8 mV, started with a $V_{1/2}$ of control of −50.81 ± 0.60 to −57.91 ± 0.43 mV after ranolazine exposure (n = 4, P < 0.05).

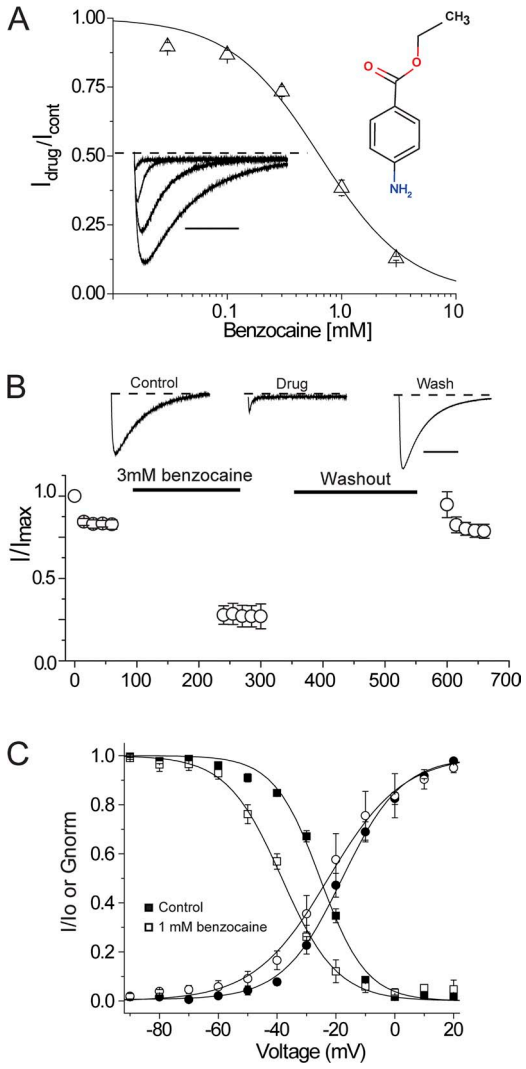

Figure 4. Blockade by the neutral drug benzocaine. (A) A benzocaine concentration response curve was generated with various benzocaine concentrations (30 µM, 100 µM, 300 µM, 1 mM, and 3 mM). The potency of benzocaine is weaker than lidocaine with an IC_{50} of 650 µM. Representative traces were obtained from 0 µM, 300 µM, 1 mM, and 3 mM benzocaine applications and are shown in the bottom inset. The dashed line indicates the zero current level. The top inset is a chemical structure of benzocaine. Bar, 500 ms. (B) 3 mM benzocaine was applied extracellularly for 3 min while holding the cells at −120 mV. Test pulse delivery and washout were performed as described in Fig. 2 C. Representative current traces are shown with the zero current lines (dotted lines). Bar, 500 ms. (C) Conductance-voltage relationship curves were generated for control (●) and for after 3 mM benzocaine (○). Similarly, SSI curves were constructed before (■) and after the exposure to 3 mM benzocaine (□). (A–C) n = 4. Error bars represent SEM.

As the concentration of each of the compounds was increased, there were two effects on NaChBac current: an instantaneous decrease in the peak current and an apparent speeding in the inactivation rate of the current. The concentration-dependent increase in the apparent inactivation rate of the current could be explained by an on-rate of LA block that should increase linearly with the concentration of LA for a bimolecular reaction scheme. Alternatively, the increase in apparent inactivation rate could actually be a result of the blocked state of the channel having an increased probability of inactivating. In support of the latter possibility, the rate of inactivation did not increase linearly with concentration but saturated with a similar concentration to the maximal block concentration (Fig. 6). The rates of inactivation were well fit for lidocaine and benzocaine with a three-state model in which inactivation into an absorbing inactivated state was more rapid from the blocked state (Fig. 6 D). In this model, K represents the experimentally determined equilibrium block equal to the IC_{50}, k_{OI} represents the rate of NaChBac inactivation measured in the absence of LA, and k_{BI} represents the rate of inactivation from the LA-bound state. The concentration dependence of the inactivation rate is then described by $\rho_i = k_{OI} \times (1 - P_B) + k_{BI} \times P_B$, where $P_B = 1/(1 + K/[LA])$ is the equilibrium probability that the channel is blocked. In this model, k_{OI} and P_B are determined experimentally. The model was fit to the mean data, giving fitted parameters (±SEM of the fitting) of k_{BI} = 0.0046 ± 0.0005 s^{-1} for lidocaine (where k_{OI} = 0.0015 s^{-1}) and 0.0062 ± 0.0006 s^{-1} for ranolazine (where k_{OI} = 0.0015 s^{-1}), indicating that the increase of inactivation rate can be described by the LA block promoting inactivation, similar to a "spring in the door" model proposed previously for mutant *Shaker* channels (Ahern et al., 2009). For benzocaine, which showed the most dramatic speeding of

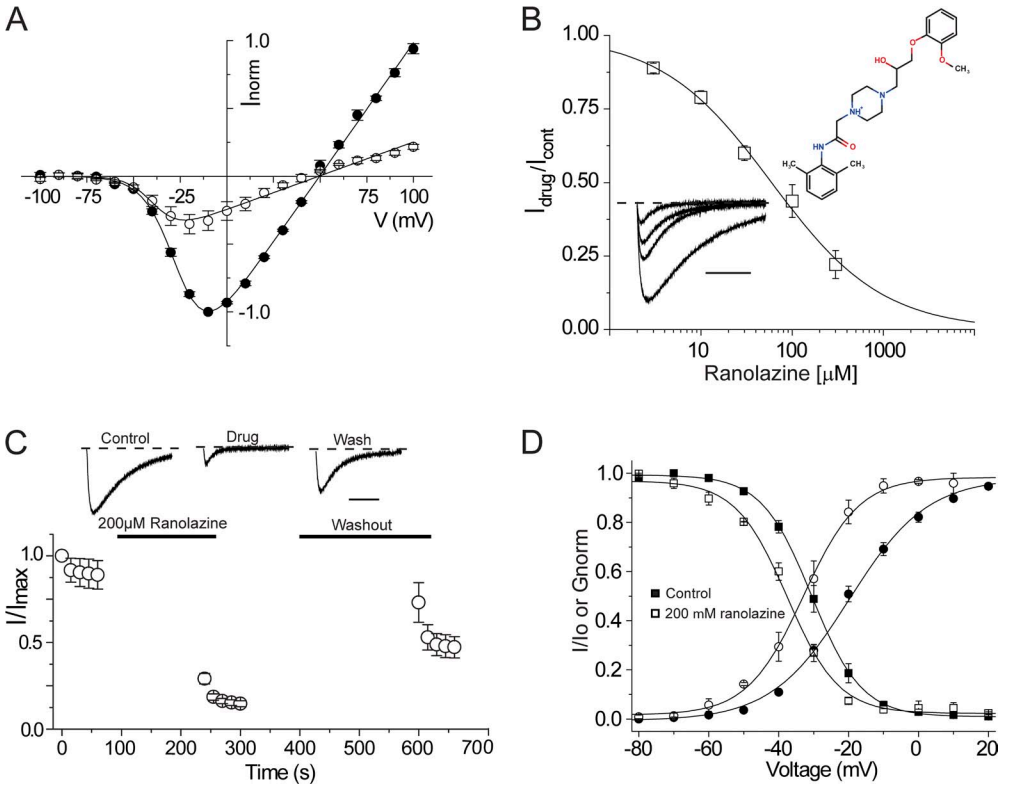

Figure 5. Inhibition by ranolazine. (A) Current-voltage relationships before (●) and after (○) the extracellular application of 200 μM ranolazine are shown. 100-ms depolarizing pulses from −100 to 100 mV with 10-mV increments at 0.1 Hz were performed before and after the drug application. $n = 3$. (B) The potency of current inhibition was the highest with ranolazine, with an IC_{50} of ∼60 μM. Representative traces are shown in the bottom inset. The dashed line indicates the zero current level. The top inset represents a chemical structure of ranolazine. (C) The diary plot of 200 μM ranolazine was constructed as described in Fig. 2 C. Representative current traces are shown with the zero current lines (dotted lines). (B and C) $n = 4$. Bar, 500 ms. (D) Effects on the conductance-voltage curve before (●) and after (○) the 200 μM ranolazine exposure. A significant left shift in the SSI curve was observed before (■) and after (□) the 200 μM ranolazine application. Error bars represent SEM.

inactivation (Fig. 6 C), the three-state model failed to fit the data well at low concentrations, as indicated by the dashed line. To account for this deviation, we considered previous work on LA block that has suggested there may be two interaction sites in the channel: a rapidly accessible low affinity site that catalyzes the entry to a higher affinity site (Gingrich et al., 1993). In our model, we conceived that the IC_{50} we measured from peak currents corresponded to the fast blocking site (BS1) that is accessed before a second site that, when occupied, promotes inactivation (BS2). This then leads to a four-state model, depicted in Fig. 6 D, in which the inactivation rate will be described by $\rho_i = k_{OI} \times [(1 - P_{BS1}) - P_{BS2}] + k_{BI} \times P_{BS1} \times P_{BS2}$.

This model fit the data well by accounting for the deviation at low concentrations (Fig. 6 C, solid line) and gave fitted parameters for k_{B2I} of $0.0184 \pm 0.0017\ s^{-1}$ and an equilibrium constant for the second site, BS2, of $K_2 = 320.1 \pm 142.7$ μM. These data suggest that LA binding to NaChBac, if we assume open channel block is primarily a fast block that reaches equilibrium faster than channel opening, has the added effect of stabilizing the inactivated state when blocking.

Next, in an attempt to further understand lidocaine block of NaChBac, we performed an extensive alanine scan of the selectivity filter and S6 segments. However, many mutations displayed nonexpressing phenotypes, including L182A, Q186A, Q186N, Q186E, V187A, T189A, L190A, E191A, W193A, W193Y, W193F, S195A, V197A, R199A, L217A, L217F, and N225A, whereas S180A, L181A, T183A, L184A, S192A, and F227A showed expression but had modest effects on channel gating. This strategy ultimately revealed an S6 mutation, T220A, shown in the homology model in Fig. 7 A, which nearly abolished inactivation in NaChBac (Fig. 7 B). This mutant displays little inactivation over a wide range of voltages, as shown in Fig. 7 C, and has a hyperpolarizing shift in the G-V relationship. Importantly for use in the study of blockers, this mutation had little impact on the overall channel affinity for lidocaine, with an IC_{50} from 260 μM to 765 μM for wild-type and T220A channels, respectively (Fig. 8 B). We aimed to use this mutant to investigate the kinetics of drug block in a channel without inactivation to more cleanly characterize the blocking kinetics in a manner akin to the domain III–IV linker IFM to QQQ mutation in eukaryotic Na_V channels. Surprisingly, application of lidocaine to the mutant produced robust inhibition with little evidence of blocking kinetics (Fig. 8 A), suggesting lidocaine acts a fast cytoplasmic blocker of NaChBac.

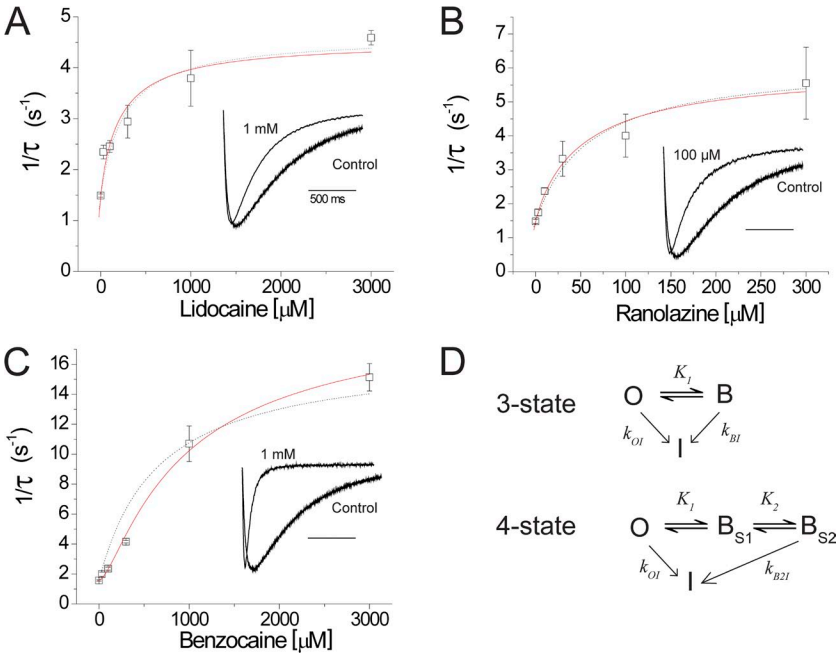

Figure 6. LA block enhances the rate of NaChBac inactivation. (A–C) Rates of NaChBac inactivation ($1/\tau$) were plotted against drug concentration for lidocaine (A), ranolazine (B), and benzocaine (C). The insets in each plot are normalized traces illustrating the increased inactivation rates when the channel is blocked. $n = 4$. (D) The three- and four-state models used to fit the increase in inactivation rate where O is the open channel, B is the channel when occupied by the blocker, and I is the inactivated state. The three-state model adequately fit the data for lidocaine and ranolazine, whereas for benzocaine the addition of an extra blocking state, BS2, from which inactivation was promoted (solid line fit in C), improved the fit at lower concentrations when compared with the three-state model (dashed line shown for comparison in C). Error bars represent SEM.

DISCUSSION

The initial cloning, subsequent characterization, and recent structural advances with bacterial sodium channels have begun to shed new understanding on these channels and how they might relate to the basic principles of sodium channel gating and pharmacology (Ren et al., 2001; Pavlov et al., 2005; Blanchet and Chahine, 2007; Blanchet et al., 2007; Irie et al., 2010; Payandeh et al., 2011; Yarov-Yarovoy et al., 2012). Up to 12 voltage-gated bacterial sodium channel genes have been discovered (Koishi et al., 2004), but it remains to be shown which aspects of NaChBac channel gating are specific to eukaryotic sodium channels and which inform on the generic features of

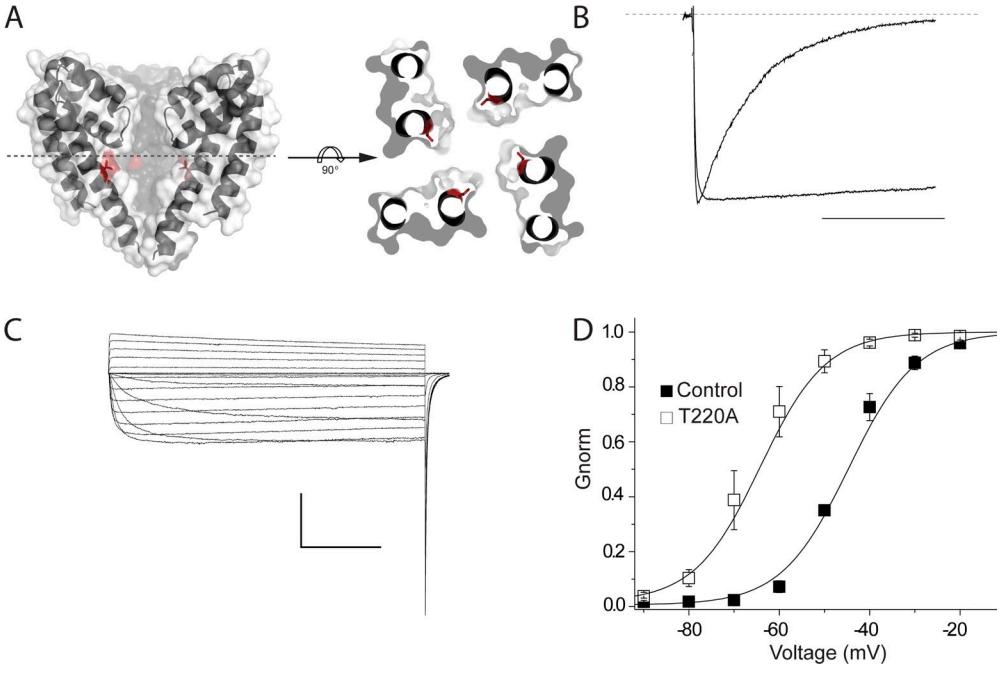

Figure 7. Characterization of a noninactivating mutant, T220A. (A) A side view of the NaChBac homology model highlighting the location of T220 of the S6 segment (left). The structure is also shown with a top view (right) that is sliced approximately through the middle of the pore from the side parallel to the membrane, then rotated 90° horizontally to highlight the orientation of T220. (B) Mutation of T220A of NaChBac has resulted in a noninactivating channel. Normalized traces of wild-type NaChBac and T220A mutant are shown. Cells were held at a holding potential of −120 mV, and channels were activated by 500 ms of depolarization pulse to −20 mV. The dashed line indicates the zero current level. Bar, 250 ms. (C) Representative current traces of T220A mutant. HEK-293 cells were held at a holding potential of −120 mV with patch-clamp configuration. NaChBac channels expressing T220A were activated by 1 s of depolarizing pulses from −100 to 0 mV in 10-mV increments. Bar: horizontal, 250 ms; vertical, 4 nA. (D) Current-voltage relationship between wild-type NaChBac and T220A mutant. A significant 20-mV left shift was observed with T220A ($V_{1/2} = -65.765 \pm 2.89$ mV; mean ± SEM, $n = 5$) as compared with wild type ($V_{1/2} = -45.52 \pm 0.90$ mV; mean ± SEM, $n = 3$), with $P < 0.01$. Error bars represent SEM.

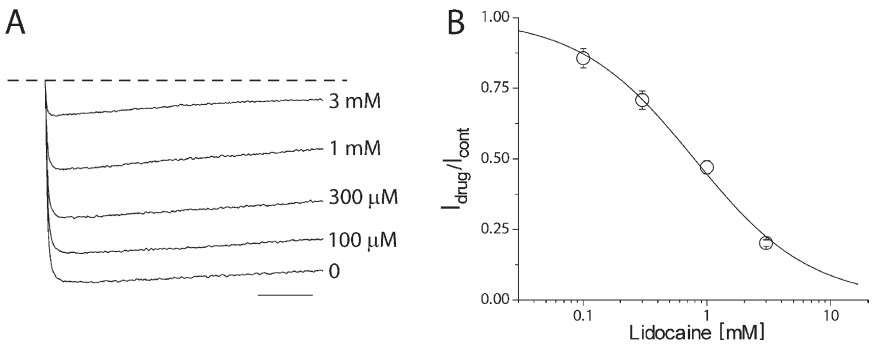

Figure 8. Lidocaine inhibition of T220A. (A) Representative current traces of T220A. The application of increasing concentrations of lidocaine to the control trace (bottom) significantly reduced the peak currents. Lidocaine was applied by a fast perfusion while applying depolarizing pulses from −120 to −20 mV for 500 ms with 3-s intervals. The dashed line indicates the zero current level. Bar, 100 ms. (B) The representative lidocaine concentration response curve describing the effects of lidocaine on T220A was generated with the mean of $I_{drug}/I_{control}$ obtained from the peak currents after exposing cells to 100 μM, 300 μM, 1 mM, and 3 mM lidocaine. The mean IC_{50} for lidocaine is 765 ± 76.3 μM, with a mean slope of 0.92 ± 0.1 ($n = 4$). Error bars represent SEM.

voltage-gated ion channels. In terms of pharmacology and channel block, NaChBac displays characteristics associated with both Na^+ and Ca^{2+} channels (Ren et al., 2001; Zhao et al., 2004), but their putative interactions with LA molecules have yet to be fully described. We therefore studied the pharmacology of NaChBac channels in the *Xenopus* oocyte, as this system provided a simple platform for the rapid screening of compounds, and, importantly, current expression was stable and channels behaved functionally in a similar fashion to a previous study (Ren et al., 2001). We show that NaChBac is blocked by the classical LA lidocaine with an apparent affinity of 260 μM. In each instance, the rapid reduction in current after drug application was likely not caused by spurious loss of current because under our recording conditions little rundown is displayed after a modest initial current decrease. Moreover, after a brief washout period, much of the blocked current was restored to control levels (Fig. 2 C). Lidocaine exposure also resulted in a hyperpolarizing, leftward shift in the SSI relationship, thus recapitulating an experimental hallmark of lidocaine block of mammalian Na_V channels. We also extended our observations to the cardiac sodium channel drug ranolazine, a lidocaine derivative that has an apparent preference for preopen channels (Antzelevitch et al., 2011). This drug showed the highest NaChBac potency with an approximately fourfold lower K_d of 60 μM compared with lidocaine.

In each case, drug application produced an initial rapid decrease in peak current followed by a speeding in the relaxation of the current kinetics, an effect that is reminiscent of LA block of eukaryotic sodium channels once fast inactivation has been removed, thus exposing the underlying blocking kinetics (Gingrich et al., 1993; Grant et al., 2000; Ramos and O'Leary, 2004). One explanation for this behavior is that the rapid reduction of current represents the tonic or resting blocking produced by a rapid, low affinity interaction with the channel, and the further relaxation of current represents the pseudo on-rate for entry into a high affinity site. To better understand both effects in NaChBac channels, we turned to a novel mutation, T220A, that we have identified to drastically impede channel inactivation. In particular, we aimed to see if we could separate the blocking kinetics from channel inactivation. In this regard, there was no evidence of blocking kinetics at concentrations near the IC_{50} of the T220A channel even though the mutant channels were still well blocked, strongly suggesting that lidocaine acts as a fast blocker of NaChBac. This possibility is further supported by the

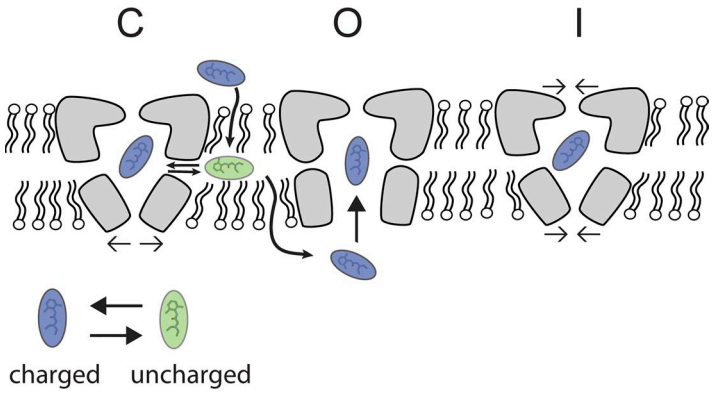

Figure 9. Model of LA block of NaChBac. LAs may gain entry by hydrophobic pathways or via rapid open channel block. Either option would be reflected in the absence of obvious blocking kinetics in the T220A mutant. Once bound, the data suggest that blockers enhance channel inactivation through an unknown mechanism. C, closed channel; O, open channel; I, inactivated channel.

observation that when QX-314 is injected directly into oocytes expressing NaChBac, currents are reduced instantaneously upon opening. What, then, could account for the apparent increase in the inactivation kinetics observed in wild-type channels? We suggest that blocker occupation of the inner vestibule enhances entry into the inactivated state, a possibility that can be accounted for with the model proposed in Fig. 6. The inactivation mechanism of bacterial sodium channels is not yet known, but one possibility is that the blocker promotes reclosure or slippage of the S6 gate similar to HCN (hyperpolarization activated cyclic nucleotide gated) channels (Shin et al., 2004). Alternatively, the blocker could effect ion occupation in the selectivity filter, which, in turn, could promote conformational changes that reduce conductance (Baukrowitz and Yellen, 1996). Regardless of the mechanism, the data and modeling support a mechanism in which LAs act as fast open channel blockers that enhance channel inactivation.

The results from NaChBac interactions with lidocaine derivatives support the working model shown in Fig. 9. The data show that external application of QX-314 has no effect on current levels, whereas internal injection results in rapid blockade, suggesting the existence of an internal blocking site and that the hydrophobic membranous pathways bar the passage of charged molecules. Once bound, the blocker effects inactivation through an unknown mechanism. However, interactions between neutral species of LAs could also effect channel gating through interactions in the membrane with other channel domains, such as the voltage sensor (Hanck et al., 2009; Muroi and Chanda, 2009).

Lidocaine has been shown to block a variety of channel types, including K_{ATP}, K2P, and nicotinic acetylcholine receptors, which show IC_{50} estimates of 43 µM, 1 mM, and 73 µM, respectively (Olschewski et al., 1996; Kindler et al., 2003; Alberola-Die et al., 2011). However, NaChBac affinity for lidocaine also approximates the resting block of cardiac sodium channels with an IC_{50} of 226 µM (Chahine et al., 1992). At present, it is not known which aspects of the block of NaChBac described here will shed new light on the mechanism of eukaryotic Na_V interactions with LAs. In regard to the possibility of functional fenestrations that might serve as drug access routes, the data suggest that NaChBac is quite different from eukaryotic Na_Vs. In particular, it has been shown that QX-314 applied externally can enter cardiac, but not neuronal, sodium channels, and introduced mutations to residues homologous to side chains that abut the bacterial fenestrations can impact this entry. However, our experiments show that QX-314 applied externally has no effect on current levels, suggesting that if such fenestrations are present in NaChBac, they are functionally divergent from cardiac Na_Vs. Nonetheless, in both bacterial and eukaryotic Na_V channels, unlike potassium channels, many key mechanistic details remain unresolved on the effects of blockers on the Na_V S6 gates and of drug modulation of inactivation. Thus, future determination of the details of NaChBac inactivation is a prerequisite for the comparison to eukaryotic Na_Vs.

Kenton J. Swartz served as editor.

Submitted: 30 January 2012
Accepted: 7 May 2012

REFERENCES

Ahern, C.A., A.L. Eastwood, D.A. Dougherty, and R. Horn. 2009. An electrostatic interaction between TEA and an introduced pore aromatic drives spring-in-the-door inactivation in Shaker potassium channels. *J. Gen. Physiol.* 134:461–469. http://dx.doi.org/10.1085/jgp.200910260

Alberola-Die, A., J. Martinez-Pinna, J.M. González-Ros, I. Ivorra, and A. Morales. 2011. Multiple inhibitory actions of lidocaine on Torpedo nicotinic acetylcholine receptors transplanted to *Xenopus* oocytes. *J. Neurochem.* 117:1009–1019. http://dx.doi.org/10.1111/j.1471-4159.2011.07271.x

Antzelevitch, C., A. Burashnikov, S. Sicouri, and L. Belardinelli. 2011. Electrophysiologic basis for the antiarrhythmic actions of ranolazine. *Heart Rhythm.* 8:1281–1290. http://dx.doi.org/10.1016/j.hrthm.2011.03.045

Baukrowitz, T., and G. Yellen. 1996. Use-dependent blockers and exit rate of the last ion from the multi-ion pore of a K+ channel. *Science.* 271:653–656. http://dx.doi.org/10.1126/science.271.5249.653

Blanchet, J., and M. Chahine. 2007. Accessibility of four arginine residues on the S4 segment of the *Bacillus halodurans* sodium channel. *J. Membr. Biol.* 215:169–180. http://dx.doi.org/10.1007/s00232-007-9016-1

Blanchet, J., S. Pilote, and M. Chahine. 2007. Acidic residues on the voltage-sensor domain determine the activation of the NaChBac sodium channel. *Biophys. J.* 92:3513–3523. http://dx.doi.org/10.1529/biophysj.106.090464

Chahine, M., L.Q. Chen, R.L. Barchi, R.G. Kallen, and R. Horn. 1992. Lidocaine block of human heart sodium channels expressed in *Xenopus* oocytes. *J. Mol. Cell. Cardiol.* 24:1231–1236. http://dx.doi.org/10.1016/0022-2828(92)93090-7

Gingrich, K.J., D. Beardsley, and D.T. Yue. 1993. Ultra-deep blockade of Na+ channels by a quaternary ammonium ion: catalysis by a transition-intermediate state? *J. Physiol.* 471:319–341.

Grant, A.O., R. Chandra, C. Keller, M. Carboni, and C.F. Starmer. 2000. Block of wild-type and inactivation-deficient cardiac sodium channels IFM/QQQ stably expressed in mammalian cells. *Biophys. J.* 79:3019–3035. http://dx.doi.org/10.1016/S0006-3495(00)76538-6

Hanck, D.A., E. Nikitina, M.M. McNulty, H.A. Fozzard, G.M. Lipkind, and M.F. Sheets. 2009. Using lidocaine and benzocaine to link sodium channel molecular conformations to state-dependent antiarrhythmic drug affinity. *Circ. Res.* 105:492–499. http://dx.doi.org/10.1161/CIRCRESAHA.109.198572

Hille, B. 1977. Local anesthetics: hydrophilic and hydrophobic pathways for the drug-receptor reaction. *J. Gen. Physiol.* 69:497–515. http://dx.doi.org/10.1085/jgp.69.4.497

Irie, K., K. Kitagawa, H. Nagura, T. Imai, T. Shimomura, and Y. Fujiyoshi. 2010. Comparative study of the gating motif and C-type inactivation in prokaryotic voltage-gated sodium channels. *J. Biol. Chem.* 285:3685–3694. http://dx.doi.org/10.1074/jbc.M109.057455

Kimbrough, J.T., and K.J. Gingrich. 2000. Quaternary ammonium block of mutant Na+ channels lacking inactivation: features of a transition-intermediate mechanism. *J. Physiol.* 529:93–106. http://dx.doi.org/10.1111/j.1469-7793.2000.00093.x

Kindler, C.H., M. Paul, H. Zou, C. Liu, B.D. Winegar, A.T. Gray, and C.S. Yost. 2003. Amide local anesthetics potently inhibit the human tandem pore domain background K+ channel TASK-2 (KCNK5). *J. Pharmacol. Exp. Ther.* 306:84–92. http://dx.doi.org/10.1124/jpet.103.049809

Koishi, R., H. Xu, D. Ren, B. Navarro, B.W. Spiller, Q. Shi, and D.E. Clapham. 2004. A superfamily of voltage-gated sodium channels in bacteria. *J. Biol. Chem.* 279:9532–9538. http://dx.doi.org/10.1074/jbc.M313100200

Muroi, Y., and B. Chanda. 2009. Local anesthetics disrupt energetic coupling between the voltage-sensing segments of a sodium channel. *J. Gen. Physiol.* 133:1–15. http://dx.doi.org/10.1085/jgp.200810103

Olschewski, A., M.E. Bräu, H. Olschewski, G. Hempelmann, and W. Vogel. 1996. ATP-dependent potassium channel in rat cardiomyocytes is blocked by lidocaine. Possible impact on the antiarrhythmic action of lidocaine. *Circulation.* 93:656–659.

Pavlov, E., C. Bladen, R. Winkfein, C. Diao, P. Dhaliwal, and R.J. French. 2005. The pore, not cytoplasmic domains, underlies inactivation in a prokaryotic sodium channel. *Biophys. J.* 89:232–242. http://dx.doi.org/10.1529/biophysj.104.056994

Payandeh, J., T. Scheuer, N. Zheng, and W.A. Catterall. 2011. The crystal structure of a voltage-gated sodium channel. *Nature.* 475:353–358. http://dx.doi.org/10.1038/nature10238

Ramos, E., and M.E. O'Leary. 2004. State-dependent trapping of flecainide in the cardiac sodium channel. *J. Physiol.* 560:37–49. http://dx.doi.org/10.1113/jphysiol.2004.065003

Ren, D., B. Navarro, H. Xu, L. Yue, Q. Shi, and D.E. Clapham. 2001. A prokaryotic voltage-gated sodium channel. *Science.* 294:2372–2375. http://dx.doi.org/10.1126/science.1065635

Schwarz, W., P.T. Palade, and B. Hille. 1977. Local anesthetics. Effect of pH on use-dependent block of sodium channels in frog muscle. *Biophys. J.* 20:343–368. http://dx.doi.org/10.1016/S0006-3495(77)85554-9

Shin, K.S., C. Maertens, C. Proenza, B.S. Rothberg, and G. Yellen. 2004. Inactivation in HCN channels results from reclosure of the activation gate: desensitization to voltage. *Neuron.* 41:737–744. http://dx.doi.org/10.1016/S0896-6273(04)00083-2

Yang, N., A.L. George Jr., and R. Horn. 1996. Molecular basis of charge movement in voltage-gated sodium channels. *Neuron.* 16:113–122. http://dx.doi.org/10.1016/S0896-6273(00)80028-8

Yarov-Yarovoy, V., P.G. DeCaen, R.E. Westenbroek, C.Y. Pan, T. Scheuer, D. Baker, and W.A. Catterall. 2012. Structural basis for gating charge movement in the voltage sensor of a sodium channel. *Proc. Natl. Acad. Sci. USA.* 109:E93–E102. http://dx.doi.org/10.1073/pnas.1118434109

Yue, L., B. Navarro, D. Ren, A. Ramos, and D.E. Clapham. 2002. The cation selectivity filter of the bacterial sodium channel, NaChBac. *J. Gen. Physiol.* 120:845–853. http://dx.doi.org/10.1085/jgp.20028699

Zhao, Y., T. Scheuer, and W.A. Catterall. 2004. Reversed voltage-dependent gating of a bacterial sodium channel with proline substitutions in the S6 transmembrane segment. *Proc. Natl. Acad. Sci. USA.* 101:17873–17878. http://dx.doi.org/10.1073/pnas.0408270101